COMPDYN 2011
III ECCOMAS Thematic Conference on
Computational Methods in Structural Dynamics and Earthquake Engineering
M. Papadrakakis, M. Fragiadakis, V. Plevris (eds.)
Corfu, Greece, 25–28 May 2011

THEORETICAL EVALUATION OF YIELDING SHEAR PANEL DEVICE FOR PASSIVE ENERGY DISSIPATION

Md Raquibul Hossain [1], Mahmud Ashraf [2] and Faris Albermani [3]

[1] School of Civil Engineering, The University of Queensland
St Lucia, QLD 4072, Australia
md.hossain@uqconnect.edu.au

[2] School of Civil Engineering, The University of Queensland
St Lucia, QLD 4072, Australia
m.ashraf@uq.edu.au

[3] School of Civil Engineering, The University of Queensland
St Lucia, QLD 4072, Australia
f.albermani@uq.edu.au

Keywords: Earthquake, Passive Energy Dissipation, Shear deformation, Tri-linear model, Yielding Shear Panel Device.

Abstract. *Metal yielding devices have been used in structures for decades to absorb earthquake energy whereby damages to the major structural components could be minimised. A recent technique to exploit the shear deformation of thin metal plates to dissipate energy has given rise to a new yielding shear panel device (YSPD); a thin steel plate is welded within steel a square hollow section (SHS)to form the device. Laboratory test results showed the potential of YSPD in energy dissipation. The behaviour of YSPD is determined by a complex interaction among the thin diaphragm plate, the surrounding SHS and the boundary conditions i.e. the structural elements that connect the device to the parent structure. This paper investigates the load-deformation response of YSPD and proposes a theoretical model to predict the experimental behaviour using the knowledge of the geometry of YSPD and the properties of the material. Previously proposed analytic method based only on the shear deformation of the diaphragm plate is revisited; appropriate modifications are proposed to include the effects of the deformations observed in the SHS and the obvious rotation of the loading plate. A tri-linear load-deformation model is proposed herein and the predictions obtained from the numerical models are compared with the available test results.*

1 INTRODUCTION

Earthquakes cause significant damages to structures resulting in either complete demolition or the affected structures require complex and expensive rehabilitation techniques to be serviceable. Minimization of structural damages due to earthquake is a major area of research which contributed to the development of a number of active, semi-active and passive control mechanisms during the last few decades. The current research investigates the structural performance of a newly proposed yielding shear panel device (YSPD) for passive energy dissipation. YSPD is simple to manufacture and is economical when compared against currently available devices. Tests carried out on the device demonstrate its potential for considerable energy absorption [1]. Hossain et. al. [2] developed finite element models and verified their performance against available monotonic and cyclic test results. An appropriate theoretical model for YSPD is required to understand the effects of this device by analysing structures including different YSPDs. Current paper proposes a tri-linear force-displacement model for YSPD, which is verified against the results obtained from tests and finite element simulation.

2 YIELDING SHEAR PANEL DEVICE (YSPD)

Diagonal tension field that develops in the post-buckling regime of a thin steel plate under shear offers significant strength and ductility and hence can be utilized to dissipate energy. This concept led to the development of a new metallic passive energy dissipating device 'Yielding Shear Panel Device' (YSPD). YSPD was introduced by Williams and Albermani [3] based on the design proposed by U. Dorka at the University of Kassel, Germany to exploit the energy dissipative capability of steel plates through in-plane shear deformation and the concept was further explored by Schmidt et.al. [4] and Williams and Albermani [5]. YSPD relies on the in-plane shear deformation of a thin diaphragm steel plate welded inside a square hollow section (SHS). This device can be placed beneath a structural beam using a V-braceso that it automatically comes into play in the event of any horizontal excitation. Figure 1 shows a typical assembly for YSPD.

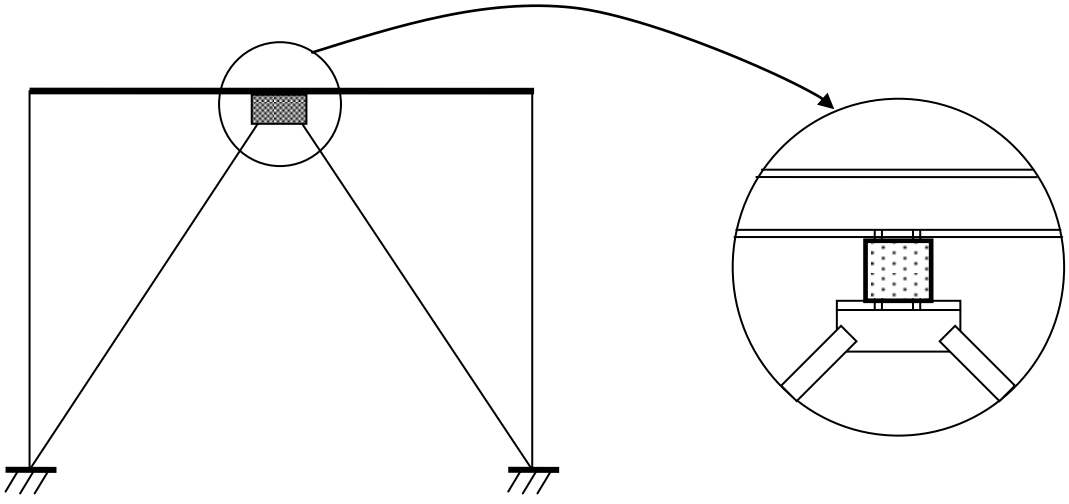

Figure 1: Typical YSPD-brace assembly.

Chan et. al. [1] conducted a series of monotonic and cyclic tests using various plate thicknesses and device configurations for YSPD. The tested specimens were fabricated using a short segment of a square hollow section (SHS) with a steel diaphragm plate welded inside, as shown in Figure 2. Four bolt holes spaced at a centre-to-centre distance 's' were drilled on

each of the two opposite SHS flanges for connecting the device to the test setup; this connection is analogous to the practical assembly where YSPDs are proposed to be connected using bolts to ensure easy installation and replacement. The SHS provides a boundary to the diaphragm plate so that shear forces can be applied to the plate, in addition to providing necessary detail for connections to the parent structural frame. Most importantly, the SHS serves as a boundary element allowing the tensile strips to be formed and the tension field to be developed following the post-buckling of the thin diaphragm plate. As a result of sufficiently large displacements occurring in the diaphragm plate, the input energy originating from an earthquake could be dissipated through plastic deformation.

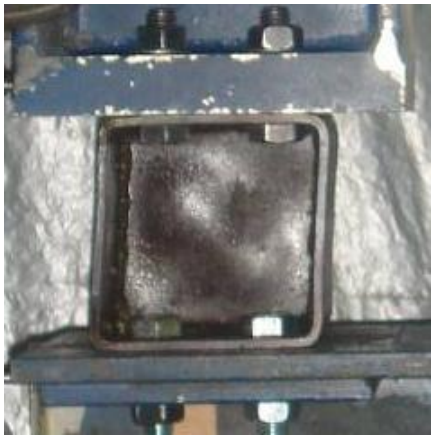

(a)

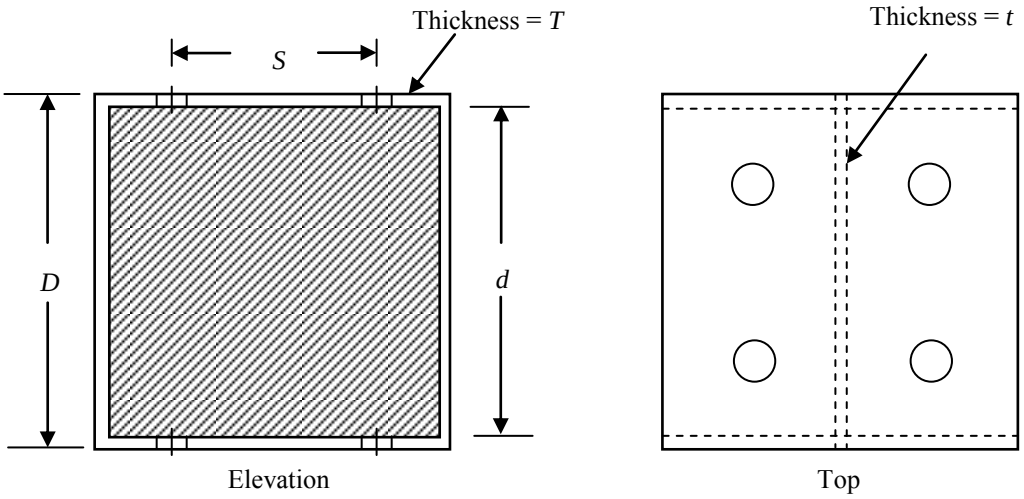

(b)

Figure 2: (a) Yielding shear panel device (YSPD) (b) Schematic diagram showing the geometric parameters of YSPD [6].

Chan et. al. [1] tested two different sizes of YSPD, 100mm × 100mm and 120mm × 120mm, with three different thickness of 2 mm, 3 mm and 4 mm for the diaphragm plate. Bolt spacing of 50 mm was used for four M16 bolts on each side of the SHS to install the test specimen between a ground beam and L-beam. The geometric dimensions of the test specimens are given in Table 1 and the reported material properties are summarized in Table 2.

YSPD Designation (D × D × t)	Diaphragm Thickness, t (mm)	SHS Size, D (mm)	SHS Thick-ness, T (mm)	Bolt Spacing, S (mm)
100×100×2	1.86	100	3.76	50
100×100×3	2.83	100	3.76	50
100×100×4	3.78	100	3.76	50
120×120×2	1.86	120	4.91	50
120×120×3	2.83	120	4.91	50
120×120×4	3.78	120	4.91	50

Table 1: Geometric details of YSPD test specimens [1]

YSPD Designation (D × D × t)	Tensile Yield Strength (MPa)	
	Diaphragm Plate	SHS
100×100×2	211.3	414.9
100×100×3	321.3	414.9
100×100×4	351.2	414.9
120×120×2	211.3	333.3
120×120×3	321.3	333.3
120×120×4	351.2	333.3

Table 2: Material properties of the test specimens [1]

3 ANALYTICAL EVALUATION OF YSPD BY CHAN ET. AL. [1]

Chan et. al. [1] classified YSPDs into two different categories based on the slenderness ratio of the diaphragm plate for theoretical evaluation. Material stress-strain response was considered elastic, perfectly-plastic with a von Mises yield criterion. Diaphragm plates were assumed to be simply supported by the SHS and were classified as either compact or slender depending on whether or not the critical shear buckling stress τ_{cr} exceeds the material yielding stress. The critical shear stress for a simply supported plate is given by [7],

$$\tau_{cr} = k_e \frac{\pi^2 E}{12(1-\nu^2)} \left(\frac{t}{d}\right)^2 \quad (1)$$

where k_e is a coefficient which depends on the aspect ratio and end restraints of the plate e.g. k_e is equal to 9.34 for square pates, whilst E and ν are Young's modulus and Poisson's ratio respectively. It is worth mentioning that the specimens used in the testing program fall within the category of YSPD with compact diaphragm plate.

Assuming an insignificant contribution from SHS, Chan et. al. [1] proposed the theoretical elastic in-plane lateral stiffness of the YSPD, k_{YSPD}as

$$k_{YSPD} = Gt \quad (2)$$

where G is the shear modulus of steel and t is the thickness of the diaphragm plate. For a device with compact diaphragm plate, the yield shear strength of YSPD is,

$$F_y = \frac{f_y}{\sqrt{3}} td \quad (3)$$

where d is the width of the steel plate and f_y is the yield strength in tension. Hence the yield displacement of the device becomes,

$$u_y = \frac{F_y}{k_{YSPD}} = \frac{f_y d}{\sqrt{3} G} \quad (4)$$

Figure 3 shows a comparison between the test result and the theoretical predictions proposed by Chan et al [1] for the load-deformation response of YSPD 100×100×4. This comparison clearly demonstrates that there is room for further modifications to the proposed theoretical model. The current research aims to develop FE models and to exploit the numerical results to propose more reliable analytic predictions for the load-deformation response of YSPD.

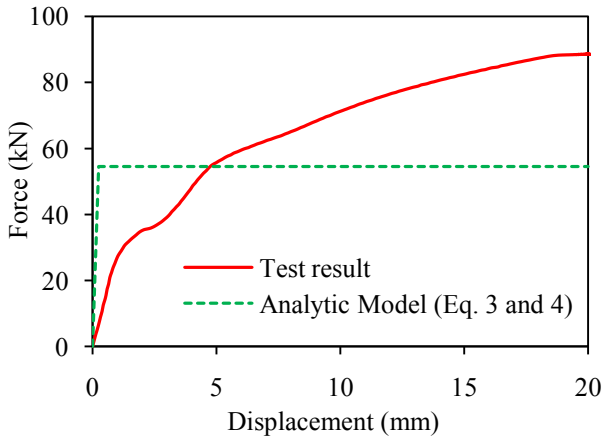

Figure 3. Comparison between the test result and the predicted force-displacement response of YSPD 100×100×4 based on the model proposed by Chan et al. [1].

4 ANALYTIC FORMULATION OF YSPD

YSPD specimens used in the laboratory testing had compact diaphragms and hence the current paper proposes analytic modelling techniques for such YSPDs so that the proposed model can be verified against test results. Size of the considered YSPDs varies within 100 to 120 mm to avoid the chance of developing large eccentric moment. Development of a trilinear load-deformation model for YSPD is described in the following sections.

4.1 Evaluation of initial stiffness

When subjected to loading, the YSPD has to resist two equal and opposite forces acting through the bolted connections and hence its initial stiffness would be equal to the force required to produce unit horizontal displacement at the loaded flange. The diaphragm plate and the SHS deform simultaneously due to the applied deformation as shown in Figure 4.

The loading and the supporting ends are assumed to remain parallel for preliminary calculations. The resulting stiffness of YSPD can be obtained by combining the individual stiffness of two constituent elements i.e. the SHS and the diaphragm. Firstly the stiffness of the diaphragm plate is formulated assuming it to be simply supported by the SHS and the diaphragm plate is assumed to deform due to pure shear. In the next step, the stiffness of the SHS is calculated assuming that the diaphragm plate deforms due to in-plane compression. The vertical flanges are also compressed as a result of the flexural deformation of the bolted flanges. The overall stiffness of the YSPD may thus be obtained as follows,

$$\frac{1}{k_{YSPD}} = \frac{1}{k_{dia}} + \frac{1}{k_{shs}} \tag{5}$$

where, k_{YSPD} = Stiffness of YSPD
k_{dia} = Stiffness of the diaphragm
k_{shs} = Stiffness of the SHS

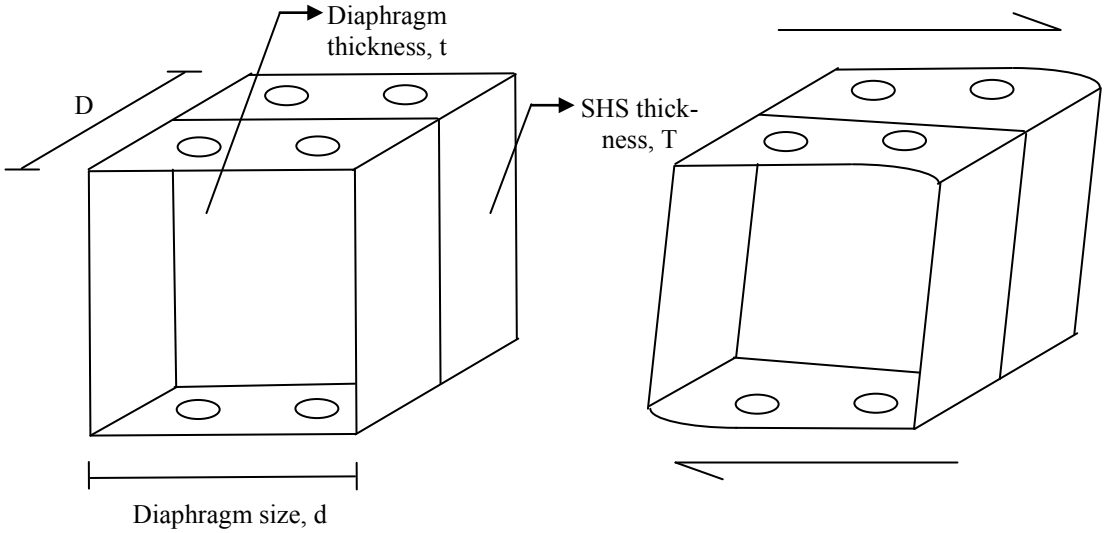

Figure 4. Undeformed and deformed shapes of a yielding shear panel device (YSPD).

4.1.1. Stiffness of the diaphragm plate

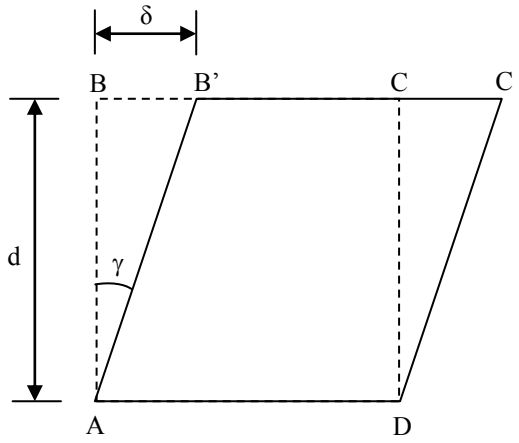

Figure 5. Undeformed Pure shear deformation of diaphragm plate.

For a unit displacement ($\delta = 1$) of the diaphragm plate (Figure 5), B is displaced to B' and the shear stain is given by,

$$\tan\gamma = \frac{\delta}{d} = \frac{1}{d} \tag{6}$$

Considering small strain, it can be reduced to,

$$\gamma = \frac{\delta}{d} = \frac{1}{d} \tag{7}$$

For elastic deformation, the shear stress,

$$\tau = G\gamma = \frac{G}{d} \tag{8}$$

Hence the elastic stiffness of diaphragm plate in pure shear may be expressed as,

$$k_{dia} = \tau dt = Gt \tag{9}$$

4.1.2. Stiffness of the SHS

The bolted flanges of the SHS undergo flexural deformation due to the in-plane compression of the diaphragm plate and the vertical flanges,. Figure 6 shows the details of assumed deformations with acting forces F_1 and F_2.

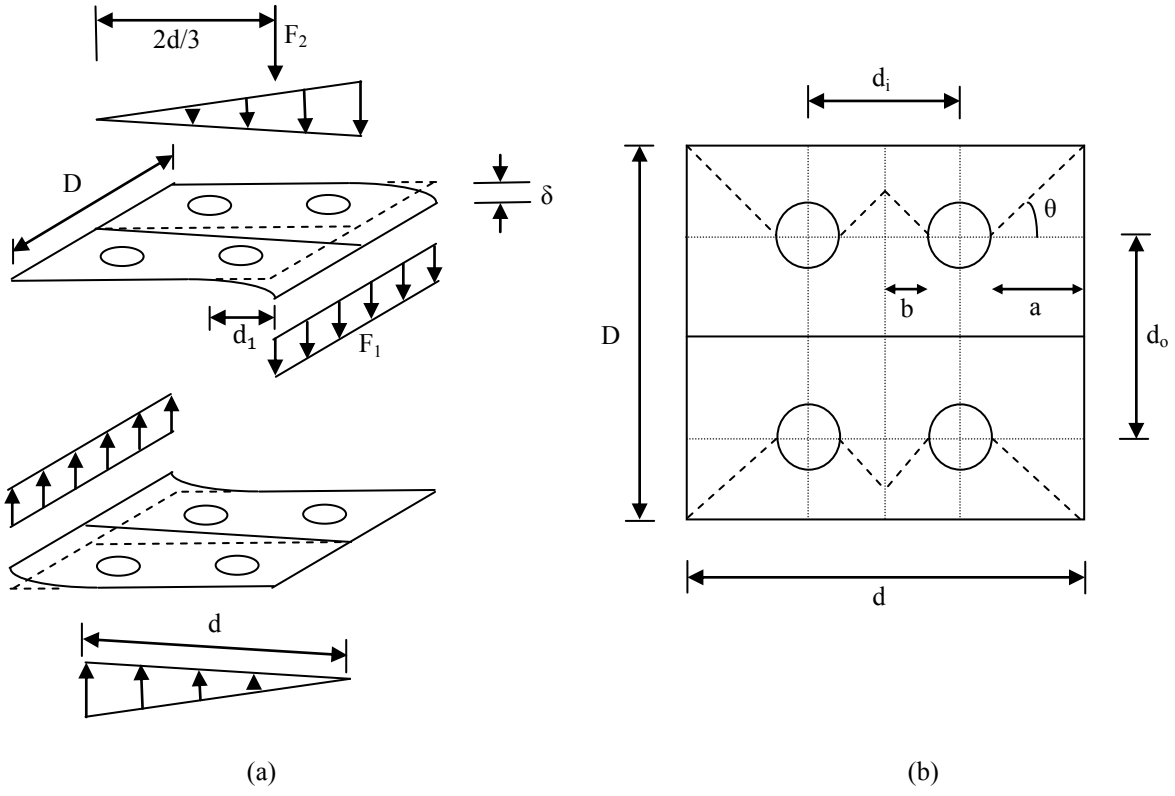

Figure 6. (a) Deformation of bolted flanges, (b) Dimensions of bolted flange.

Bolted flanges experience bending about an axis perpendicular to the loading direction due to the force F_1. By assuming a zero rotation along the line passing through the centre of nearby bolts and ignoring the effects of bolt holes we can calculate,

$$F_1 = \frac{3EI_1}{{d_1}^3} = \frac{DT^3E}{4(a+r)^3} \tag{10}$$

where, $I_1 = \frac{DT^3}{12}$

r = Radius of the bolt hole

The compression at the diaphragm plate causes deformation along the line joining the flange and the diaphragm plate. . This deformation results in an additional bending to the flange about an axis parallel to the loading direction. The acting force F_2 responsible for this deformation is assumed to have a triangular distribution due to the large in-plane rigidity of the diaphragm plate. This force may be obtained by taking strips in the flange.

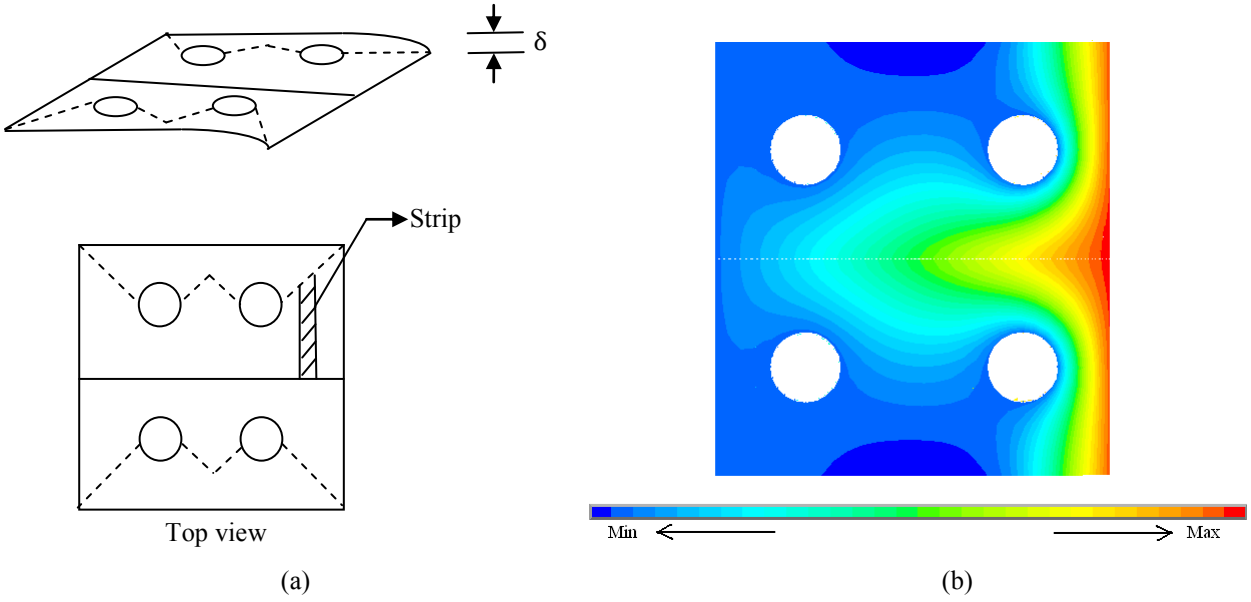

Figure 7. (a) Assumed zero rotation line on SHS flange. (b) Typical contour plot of the out of plane deformation of SHS flange

The zero rotation line is assumed as a zigzag dotted line as shown in Figure 7(a); this pattern is due to the boundary condition provided by the bolted connections. Each strip is considered to be fixed on both sides bounded by the dotted 'zero rotation' line and the line joining the diaphragm to the flange. Figure 7(b) shows a contour plot of the typical out of plane deformation of the SHS flange obtained from FE analysis [2]. The contour plot confirms that the deformation at the right part of the top flange is due to bending about both the orthogonal directions. The deformation pattern due to the compression of the diaphragm plate also verifies the assumed zigzag line for zero rotation.

The zero rotation line is assumed to make an angle of θ (Figure 6(b)) with a plane parallel to the diaphragm. The average distance (d_2) between the diaphragm line and zigzag support line can be calculated as follows,

$$d_2 = \left(\frac{d_0}{2} + \frac{a.\tan\theta}{2}\right) \times \frac{2a}{d} + \left(\frac{d_0}{2} + \frac{b.\tan\theta}{2}\right) \times \frac{2b}{d} + \left(\frac{d_0}{2} - \frac{\pi r}{4}\right) \times \frac{4r}{d}$$

$$\text{or, } d_2 = \frac{d_0}{2} + \frac{a^2.\tan\theta + b^2.\tan\theta - \pi r^2}{d} \tag{11}$$

The resultant of the triangular force considering a unit deformation at the end becomes,

$$F_2 = 2\times\left(\frac{6EI_2/d_2^3}{2}\right) = \frac{6EI_2}{d_2^3} = \frac{dT^3E}{2d_2^3} \quad (12)$$

where, $I_2 = \frac{dT^3}{12}$

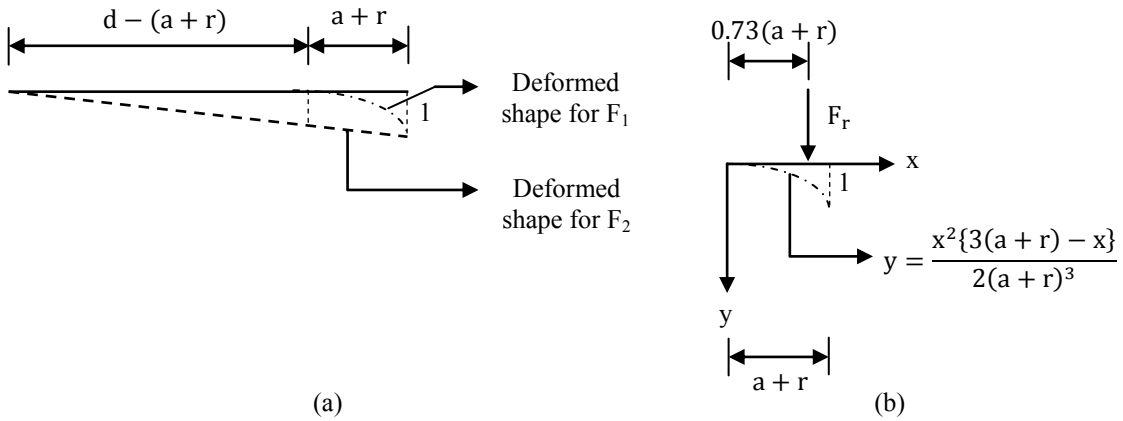

Figure 8. (a) Deformed shapes due to force F_1 and F_2 of SHS flange (b) Equation of the deformed shape for the force F_1 and reduction force F_r

A reduction in the total calculated force is required for bending moments acting at orthogonal directions. Figure 8(b) shows the deformed shape with a unit deformation at the end for F_1. The average deformation becomes 3/8 by calculating the area and dividing it with the deformed length (a+r). The common deformation due to force F_1 and F_2 are calculated. Force required to produce this common deformation is the reduction force which can be calculated as,

$$F_r = 2\times\left(\frac{6EI_3}{d_2^3}\right)\times\frac{3}{8} = \frac{3E(a+r)T^3}{8d_2^3} \quad (13)$$

where, $I_3 = \frac{(a+r)T^3}{12}$

Force F_r acts at a distance of $d_r = \{d - 0.27(a + r)\}$ from the zero deformation end.

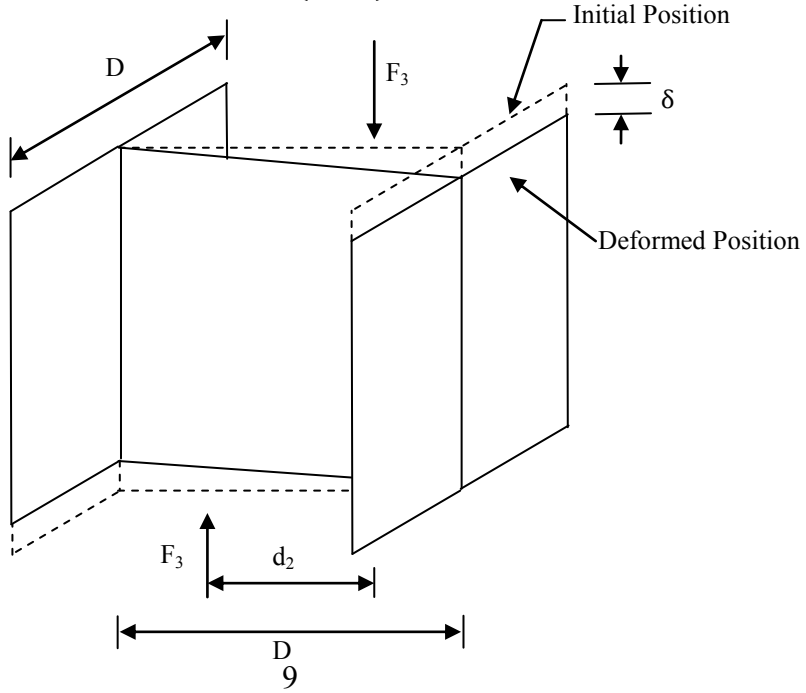

Figure 9. Compressive deformation of diaphragm plate and vertical flanges

The compression of the diaphragm plate and the vertical flanges in an YSPD is analogous to the deformation of an I-Section as shown in Figure 9. The force required to make a unit deformation i.e. strain = 1/d at the end of the flange,

$$F_3 = DT \times \frac{E}{d} + \frac{dt}{2} \times \frac{E}{d} \tag{14}$$

The distance between the zero deformation and the line of action of the force,

$$d_3 = \frac{DTE + dtE/3}{F_3} \tag{15}$$

The stiffness of the SHS can be calculated by the moment balance of these forces and thus may be expressed as follows

$$k_{SHS} = F_1 + \frac{F_2}{3} - \frac{F_r(2d_r - d)}{d} + \frac{F_3(2d_3 - d)}{d} \tag{16}$$

Calculation showed that the contribution of force F_3 is more than 98.5%. The inclination of the zero deformation angle θ, thus, has negligible effect on the overall stiffness of the SHS and hence the angle θ may be taken as 45° whilst calculating the stiffness of SHS.

4.1.3. Combined Stiffness

Test results showed considerable rotation of the loading end within the elastic range [2], which causes the stiffness of the SHS to degrade. Hence the stiffness of the SHS may be taken as ϕk_{shs}, where ϕ is a reduction factor. The modifies stiffness of YSPD (k'_{YSPD}) is thus expressed as follows,

$$\frac{1}{k'_{YSPD}} = \frac{1}{k_{dia}} + \frac{1}{\phi k_{shs}} \tag{17}$$

The value of ϕ can be determined using the initial stiffness of YSPDs obtained from the experimental investigation. Theoretical stiffness of the diaphragm plate and the SHS are calculated individually using Equations 9 and 16 ignoring the effects of rotation. Obtained stiffness magnitudes for the YSPDs and their corresponding diaphragm plates and SHS are used to plot Figure 10. The slope of the straight line is equal to $1/\phi$ according to Equation 17. The obtained value of ϕ is equal to 0.03 ignoring one outlier, which represents significantly low initial stiffness showed by YSPD 120×120×3 in the monotonic test.

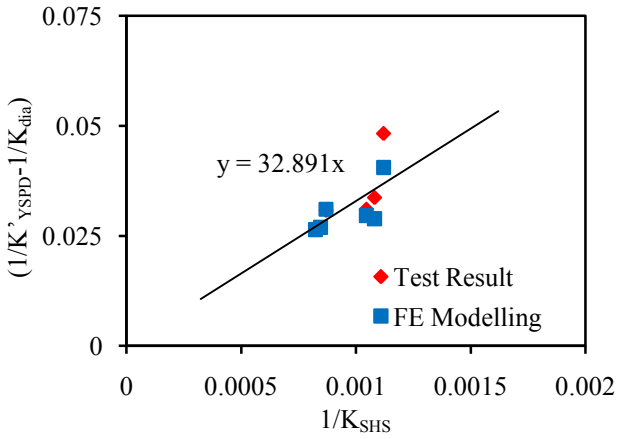

Figure 10. Stiffness plot of SHS to determine the reduction factor ϕ.

4.2 Yield Strength of YSPD

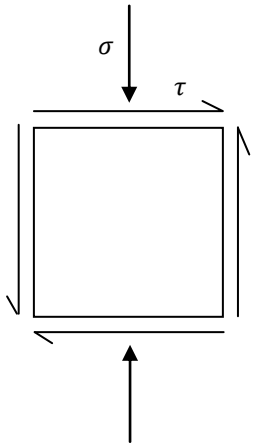

Figure 11. State of elastic stress of the diaphragm plate.

The yielding of YSPD occurs due to the combined action of axial compression and shear deformation of the diaphragm plate. The yield force and the corresponding deformation is initially calculated assuming the loading end and the support end remain parallel. The effect of support rotation is then incorporated to calculate the actual deformation. According to von Mises yield criterion,

$$\sigma_1^2 - \sigma_1\sigma_2 + \sigma_2^2 = \sigma_y^2 \tag{18}$$

where, σ_y is the tensile yield strength

$$\text{Principal stresses, } \sigma_1, \sigma_2 = -\frac{\sigma}{2} \pm \sqrt{\frac{\sigma^2}{4} + \tau^2}$$

The applied horizontal deformation δ can be divided into two components - δ_1 for the pure shear deformation of the diaphragm plate and δ_2 for the deformation of SHS. Thus,

$$\delta = \delta_1 + \delta_2 \tag{19}$$

$$\delta_1 = \frac{k_{YSPD}}{k_{dia}}\delta \tag{20}$$

$$\delta_2 = \frac{k_{YSPD}}{k_{SHS}}\delta \tag{21}$$

The resulting stresses become,

$$\tau = \frac{\delta_1 G}{d} \tag{22}$$

$$\sigma = \frac{\delta_2 E}{d} \tag{23}$$

The yield deformation δ_y can be calculated by solving Equation 18. This yield displacement changes due to the rotation of the loading end. By incorporating the effect of end rotation, yield displacement becomes,

$$\delta_y^{'} = \delta_y \frac{k_{YSPD}}{k_{YSPD}^{'}} \tag{24}$$

The yield strength of YSPD can be calculated as,

$$F_y^{'} = k_{YSPD}^{'}\delta_y^{'} \tag{25}$$

Equation 25 gives the same yield strength as calculated by Chan et. al. [1], but the initial stiffness is modified by considering the deformation of the SHS in Equation 24.

The underlying assumption of this calculation is the diaphragm plate is simply supported by the SHS. Practically the diaphragm plate is welded inside the SHS. The thickness ration of diaphragm plate and the SHS plate (t/T) determines the support rigidity. The rigidity of the support increases with the decreasing t/T ratio. Consequently, the theoretical yield strength decreases with the increasing t/T ration. Figure 12 shows the variation of the ration of theoretical yield strength and actual yield strength with the varying td^2/T. The term d^2 is used to normalize the values with different diaphragm size. The graph shows a good correlation and indicates the yield strength reduces with the increasing t/T ration.

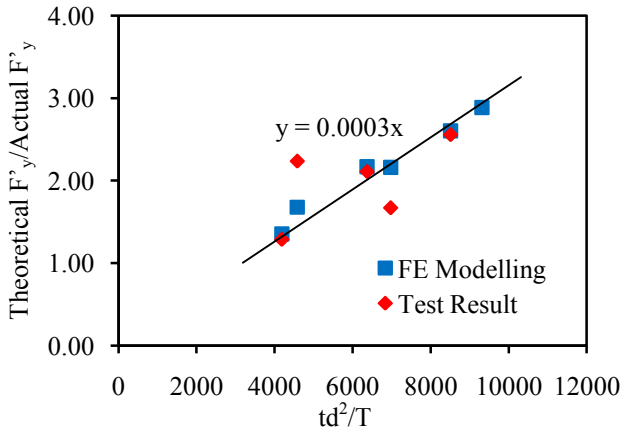

Figure 12. Correlation curve for theoretical and actual yield strength.

A strength reduction factor Ω_1 is calculated as follows,

$$\Omega_1=0.0003td^2/T \tag{26}$$

Reduced yield displacement and yield strength of YSPD becomes,

$$\delta_y^{'} = \Omega_1 \delta_y \frac{k_{YSPD}}{k_{YSPD}^{'}} \tag{27}$$

$$F_y^{'} = \Omega_1 k_{YSPD}^{'} \delta_y^{'} \tag{28}$$

4.3 Plastic Buckling Strength in Shear

Early investigations into plastic plate shear buckling were reported by Gerard [8], Stowell [9] and Bijlaard [10]. Stowell [9] and Bijlaard [10] used deformation theory for the analysis of plastic buckling of plates, whilst Gerard [8] followed the secant modulus approach. Stowell [9] derived an expression using the deformation theory and finally suggested a simplified form depending on the secant modulus of elasticity for materials with nearly constant hardening behaviour in the plastic range. Gerard [8] suggested the critical shear stress is rather dependent on the secant shear modulus. Bleich [11] proposed a simplified approximation of Stowell's plastic reduction factor using the tangent modulus concept. Later, Inoue [12] used a Tresca yield criterion [12] based modified incremental theory to analyse the plastic shear buckling of thin plates. Tugcu [13] adopted bifurcation approach to determine the effect of tensile or compressive loading on the critical buckling stress for infinitely long shear plates. Wang and Aung [14] applied the p-Ritz method for the plastic buckling analysis of thick plates based on both deformation theory and incremental theory. Alinia et al. [15] showed that incremental theory based p-Ritz method provides upper bound solutions whereas deformation theory based method predicts lower bound solutions.

Stowell [16] derived a closed form solution for determining the critical shear stress for long plates using the deformation theory. Critical buckling stress may be expressed as,

$$\tau_{cr} = k_e \frac{\pi^2 E \eta}{12(1-\nu^2)} \left(\frac{t}{d}\right)^2 \tag{29}$$

where τ_{cr} is the critical shear stress, k_e is a coefficient which depends on the aspect ratio and the end restraints of the plate, E is the Young's modulus, ν is the Poisson's ratio and η is the coefficient allowing reduction in plastic range. The coefficient ηdepends on the secant modulus of elasticity, support restraint and the plasticity behaviour of the material. For a linear hardening material Stowell [16] suggested,

$$\eta = \text{Constant}\frac{E_s}{E} \tag{30}$$

For 24S-O aluminium alloy, Stowell [16] found this constant as 0.89 for both simply supported edges and clamped edges. Bleich [11] proposed a simplified conservative approximation for the value of η as

$$\eta = \sqrt{\frac{E_t}{E}} \tag{31}$$

Gerard [8] approximated the value of η incorporating secant shear modulus G_s and shear modulus G as,

$$\eta = \frac{G_s}{G} \tag{32}$$

Gerard [8] further advanced the theory by introducing the concept of critical shear strain γ_{cr}. Using Equation 34, the critical shear strain can be found as,

$$\gamma_{cr} = k_e \frac{2(1+\nu)\pi^2}{12(1-\nu^2)} \left(\frac{t}{b}\right)^2 \tag{33}$$

The expression for critical shear strain γ_{cr} is not dependent on coefficient η and hence γ_{cr} could be easily calculated using the knowledge of the size, the slenderness ratio and the support conditions of a thin plate.

Equation 29 and 33 are used to predict the critical bucking stress and strain for the diaphragm plate and used to calculate the buckling force of a YSPD.

Real et. al. [17] presented a method to identify the critical buckling stress for a metal plate subjected to shear using finite element analysis. The bucking occurs when the stress reversal takes place in the principal stress plot; the compressive principal stress suddenly decreases once the plate starts to buckle. Finite elemnt simulation of YSPD showed the critical buckling forceis over predicted. The redused strength is resulted by the axial compressive stress acting along with the shear stress. Buckling strain is found larger in the FE model. This excessive deformation is resulted from the support rotation. Figure 13(a) shows the variation of the ratio of theoretical critical buckling strength and actual buckling strength with varying slenderness ratio (d/t). The graph shows a good correlation and the buckling strength reduction factor is calculated as,

$$\Omega_2 = 1+0.011d/t \tag{34}$$

Critical plastic buckling strain calculated according to the equation 35 can be divided into elastic and plastic parts as follows,

$$\gamma_{cr} = \gamma_{cr}^{e} + \gamma_{cr}^{p} \tag{35}$$

The multiplication factor for increasing the value of the plastic shear strain to include the effect of the support rotation depends on the plate area (td). Figure 13(b) shows the variation of the ratio of theoretical plastic shear buckling strain and actual plastic strain obtained from FE models with varying area of the diaphragm plate area (td). The graph showed a good correlation and the plastic strain multiplication factor is calculated as,

$$\Omega_3 = 0.0116td-1.81 \tag{36}$$

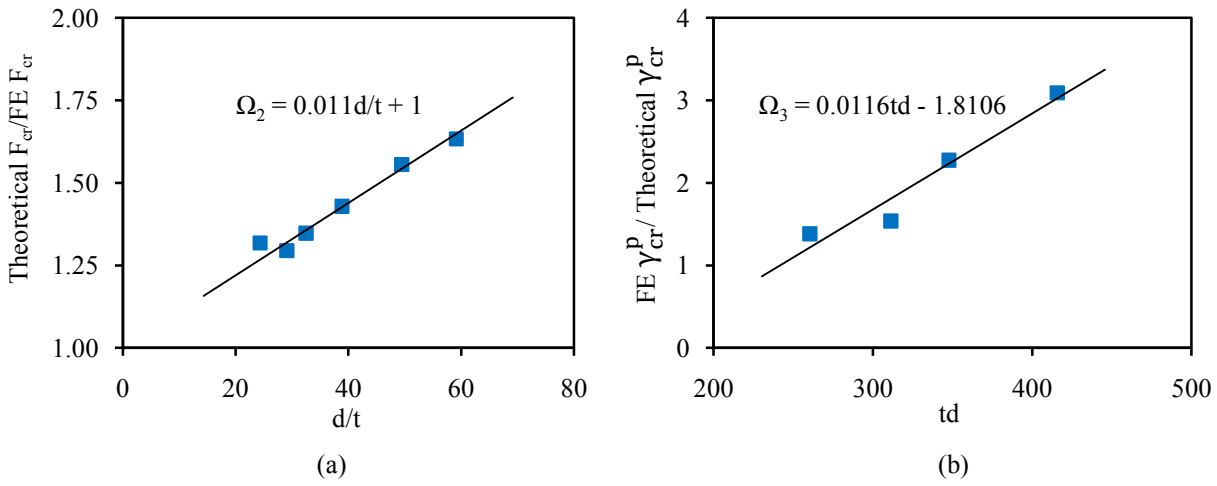

Figure 13. (a) Correlation curve for theoretical and finite element critical plastic buckling strength. (b) Correlation curve for theoretical and finite element critical plastic buckling strain.

4.4 Post Buckling Stiffness

Force-displacement response of YSPD for large deflections after the buckling of the diaphragm plate is necessary to identify its energy dissipation characteristics. A tension field is developed after the shear buckling of diaphragm plate. A typical state of stress of the diaphragm plate with a tension field inclined at an angle α is shown in Figure 14.

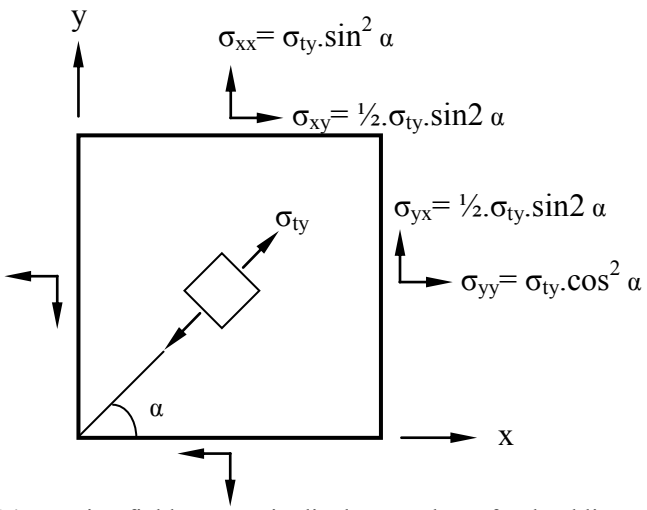

Figure 14. Tension field stresses in diaphragm plate after buckling.

The incremental shear strength of the YSPD after buckling becomes,

$$dF = ½.d\sigma_{ty}(\sin 2\alpha)td \quad (37)$$

Kharrazi [18] determined the elastic post bucking shear deformation by equating the work done by the post buckling component of the shear forces to the strain energy produced by the tension field. Kharrazi et. al. [19] extended the concept to consider hardening after reaching yield point by replacing the modulus of elasticity (E) with the tangent modulus of elasticity (E_t). Using the same technique, the incremental post buckling shear deformation becomes,

$$d\delta = 2d\sigma_{ty}.d/E_t \sin 2\alpha \quad (38)$$

Thus, the post buckling stiffness of the YSPD may be expressed as,

$$k_t = ¼.E_t \sin^2 2\alpha \quad (39)$$

Equation 39 indicates that the shear deformation behaviour after buckling depends on the inclination angle α of the tension field. A number of research works have been conducted in the last few decades to identify the angle of inclination in tension field action; Shishkin et. al. [20] summarised all available literature relevant to inclination angle. CAN/CSA-S16-01 [21] suggests a limit varying between 38° and 45° for the inclination angle of pin ended strips in steel plate walls. Shishkin et. al. [22] reported that inclination angle values between 38° to 50° gave similar results for calculating the ultimate capacity of steel plate shear walls. An inclination angle of 45° can be reasonably assumed for the tension strips developed within the square diaphragm plate of YSPD. Considering an inclination angle of 45°, the post buckling stiffness may be expressed as follows

$$k_t = ¼.E_t t \quad (40)$$

5 COMPARISON WITH TEST RESULTS AND FE MODELLING

The performance of the proposed tri-linear load deformation response is compared against those obtained from test and FE simulation. Figure 15 compares the load-deformation response for different YSPDs. The devloped FE model and analytic model with 2 mm diaphragm plate significantly underpredicts the test behaviour; this discrepancy is due to a higher strength shown by the material although the reported yield strength (211.3 N/mm^2) is unusually low.

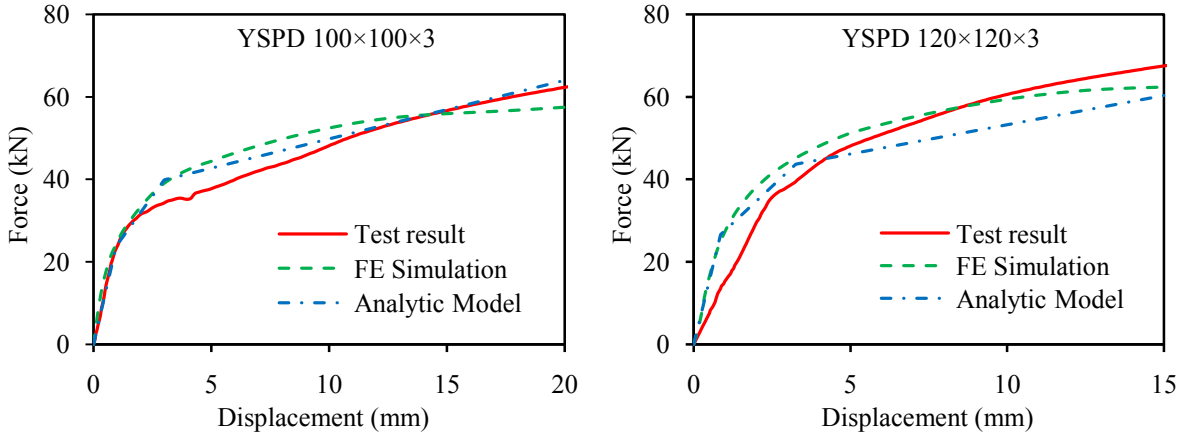

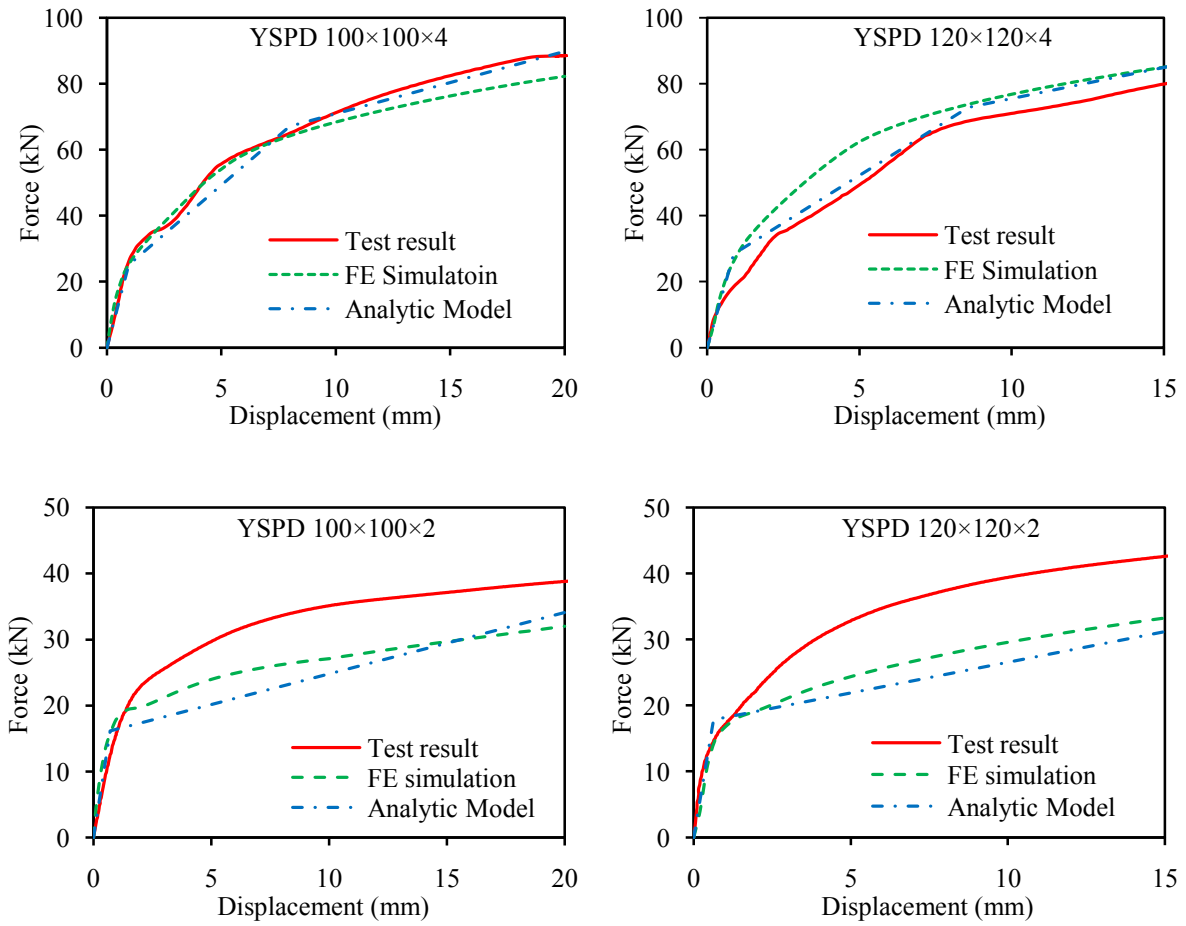

Figure 15. Force-displacement response of YSPDs.

Table 3 compares the amount of energy required to achieve specified displacements during the monotonic loading tests of YSPDs to those obtained from tri-linear models. The ratio of energy required for different displacements indicates that the developed tri-linear model can predict the required energy with reasonable accuracy.

YSPD Designation	Ratio of Energy for different displacements (Theoretical/Test)			
(D × D × t)	5 mm	10 mm	15 mm	20 mm
100×100×2	0.77	0.72	0.73	0.76
100×100×3	1.09	1.08	1.05	1.04
100×100×4	0.91	0.96	0.97	0.97
120×120×2	0.79	0.71	0.71	-
120×120×3	1.15	0.99	0.94	-
120×120X4	1.12	1.07	1.07	-

Table 3: Comparison of energy required in monotonic loading.

6 CONCLUSION

An analytic model for a newly proposed passive energy dissipation device YSPD has been presented in the current paper explaining all necessary theoretical derivations. The force-displacement response of YSPD has been idealized as a tri-linear curve. The first linear segment represents the elastic deformation; the slope of which depends on the individual stiffness of the diaphragm plate and that of the surrounding SHS in addition to the rotation of the support. Yield strength is calculated based on the yield capacity of the diaphragm plate, which is eventually reduced by introducing a yield strength reduction factor to consider the stiffness of the surrounding SHS. Second linear segment corresponds to the plastic deformation of the shear plate. Critical buckling strength is identified using Gerard's plastic buckling theory by calibrating the theoretical values using finite element results. Final linear segment represents the post buckling tension field response. Inclination of the tension field is observed not to play a significant role and hence an angle of 45^0 is adopted. Positive tangential stiffness (k_t) presents a hardening behaviour for post bucking response. The proposed theoretical model is compared with the available test results and the corresponding finite element simulations; overall, the comparisons showed good agreement. Developments of fully nonlinear theoretical formulations for YSPD are currently underway.

REFERENCES

[1] Chan, R. W. K., Albermani, F., and Williams, M. S., 2009, "Evaluation of Yielding Shear Panel Device for Passive Energy Dissipation," Journal of Constructional Steel Research, 65(2), pp. 260-268.

[2] Hossain, M. R., Ashraf, M., and Albermani, F., 2011, "Numerical Modelling of Yielding Shear Panel Device for Passive Energy Dissipation," Thin Walled Structures (Paper Submitted).

[3] Williams, M., and Albermani, F., 2003, "Monotonic and Cyclic Tests on Shear Diaphragm Dissipators for Steel Frames," Civil Engineering Bulletin No. 23, Department of Civil Engineering, University of Queensland, Australia.

[4] Schmidt, K., Dorka, U. E., Taucer, F., and Magnonette, G., 2004, "Seismic Retrofit of a Steel Frame and an Rc Frame with Hyde Systems," Institute for the Protection and the Security of the Citizen European Laboratory for Structural Assessment, European Commission Joint Research Centre.

[5] Williams, M., and Albermani, F., 2006, "Monotonic and Cyclic Tests on Shear Diaphragm Dissipators for Steel Frames," Advanced Steel Construction, 2(1), pp. 1-21.

[6] Chan, R. W. K., 2008, "Metallic Yielding Devices for Passive Dissipation of Seismic Energy," PhD Thesis, University of Queensland.

[7] Timoshenko, S., 1961, Theory of Elastic Stability, McGraw-Hill, New York.

[8] Gerard, G., 1948, "Critical Shear Stress of Plates above the Proportional Limit," Journal of Applied Mechanics-Transactions of the Asme, 15(1), pp. 7-12.

[9] Stowell, E. Z., 1948, "Critical Shear Stress of an Infinitely Long Plate in the Plastic Region," NACA Technical Note No. 1681.

[10] Bijlaard, P. P., 1949, "Theory and Tests on the Plastic Stability of Plates and Shells," Journal of the Aeronautical Sciences, 16(9), pp. 529-541.

[11] Bleich, F., 1952, Buckling Strength of Metal Structures, McGraw-Hill, New York ; London.

[12] Inoue, T., 1996, "Analysis of Plastic Buckling of Steel Plates in Shear Based on the Tresca Yield Criterion," International Journal of Solids and Structures, 33(26), pp. 3903-3923.

[13] Tugcu, P., 1998, "Effect of Axial Loading on Plastic Buckling of Long Strips under Pure Shear," Computers & Structures, 66(2-3), pp. 155-161.

[14] Wang, C. M., and Aung, T. M., 2007, "Plastic Buckling Analysis of Thick Plates Using P-Ritz Method," International Journal of Solids and Structures, 44(18-19), pp. 6239-6255.

[15] Alinia, M. M., Gheitasi, A., and Erfani, S., 2009, "Plastic Shear Buckling of Unstiffened Stocky Plates," Journal of Constructional Steel Research, doi: 10.1016/j.jcsr.2009.04.001(

[16] Stowell, E. Z., 1948, "Critical Shear Stress of an Infinitely Long Plate in the Plastic Region."

[17] Real, E., Estrada, I., and Mirambell, E., 2003, "Experimental and Numerical Investigation on Shear Response of Stainless Steel Plated Girders."

[18] Kharrazi, M., 2005, Rational Method for Analysis and Design of Steel Plate Walls, Ph.D. dissertation, University of British Columbia,Vancouver, B.C.

[19] Kharrazi, M., Ventura, C., and Prion, H., 2011, "Analysis and Design of Steel Plate Walls: Experimental Evaluation," Canadian Journal of Civil Engineering, 38(1), pp. 60-70.

[20] Shishkin, J. J., Driver, R. G., and Grondin, G. Y., 2005, Analysis of Steel Plate Shear Walls Using Modified Strip Method, Structural Engineering Rep. No. 261, Dept. of Civil Engineering, Univ. of Alberta, Alta.

[21] Can/Csa, 2001, "Csa-S16-01," Limit states design of steel structures, Canadian Standard Association, Rexdale (Ontario).

[22] Shishkin, J., Driver, R., and Grondin, G., 2009, "Analysis of Steel Plate Shear Walls Using the Modified Strip Model," Journal of Structural Engineering, 135(pp. 1357.